Saturated hydraulic conductivity model computed from bimodal water retention curves for a range of New Zealand soils

Joseph Alexander Paul Pollacco[1], Trevor Webb[1], Stephen McNeill[1], Wei Hu[2], Sam Carrick[1], Allan Hewitt[1], Linda Lilburne[1]

[1] Landcare Research, PO Box 69040, Lincoln 7640, New Zealand
[2] New Zealand Institute for Plant & Food Research Limited, Private Bag 4704, Christchurch 8140, New Zealand

Correspondence to: Joseph A.P. Pollacco (Pollacco.water@gmail.com)

Abstract. Descriptions of soil hydraulic properties, such as *soil moisture retention curve*, $\theta(h)$, and *saturated hydraulic conductivities*, K_s, are a prerequisite for hydrological models. Since the measurement of K_s is expensive, it is frequently derived from pedotransfer functions. Because it is usually more difficult to describe K_s than $\theta(h)$ from pedotransfer functions, Pollacco et al. (2013) developed a physical unimodal model to compute K_s solely from hydraulic parameters derived from the Kosugi $\theta(h)$. This unimodal K_s model, which is based on a unimodal Kosugi soil pore-size distribution, was developed by combining the approach of Hagen-Poiseuille with Darcy's law and by introducing three tortuosity parameters. We report here on (1) the suitability of the Pollacco unimodal K_s model to predict K_s for a range of New Zealand soils, and (2) further adaptations to this model to adapt it to dual-porosity structured soils for soils having aggregates by computing the soil water flux through a continuous function of an improved bimodal pore-size distribution. The improved bimodal K_s model was tested with a New Zealand data set derived from historical measurements of K_s and $\theta(h)$ for a range of soils derived from sandstone and siltstone. The K_s data were collected using a small core size of 10 cm diameter, causing large uncertainty in replicate measurements. Predictions of K_s were further improved by distinguishing topsoils from subsoil. Nevertheless, as expected stratifying the data with soil texture only slightly improved the predictions of the physical K_s models because the K_s model is based on pore-size distribution and the calibrated parameters were obtained within the physically feasible range. The improvements made to the unimodal K_s model by using the new bimodal K_s model are modest when compared to the unimodal model, which is explained by the poor accuracy of measured total porosity. Nevertheless, the new bimodal model provides an acceptable fit to the observed data. The study highlights the importance of improving K_s measurements with larger cores.

Keywords. Saturated hydraulic conductivity; Bimodal; Kosugi model; Soil moisture retention curves; Pedotransfer functions; Tortuosity; Hagen-Poiseuille; soils; New Zealand; S-map

Abbreviations. PTFs: statistical pedotransfer functions; **S-map:** New Zealand soil database; ***θ(h)*** soil moisture retention curve; $\boldsymbol{K_s}$ saturated hydraulic conductivity

1 Introduction

Modelling of the water budget, irrigation, and nutrient and contaminant transport through the unsaturated zone requires accurate soil moisture retention, *θ(h)*, and unsaturated hydraulic conductivity, *K(θ)*, curves. The considerable time and cost involved in measuring *θ(h)* and *K(θ)* directly for a range of soils mean that the information for specific soils of interest is often not available (Webb, 2003). Therefore, these curves are generally retrieved from pedotransfer functions (PTFs), which are statistical relationships that generate lower-precision estimates of physical properties of interest based on many rapid and inexpensive measurements (e.g. Balland and Pollacco, 2008; Pollacco, 2008; Anderson and Bouma, 1973; Webb, 2003, Cichota et al., 2013).

The S-map database (Lilburne et al., 2012; Landcare Research, 2015) provides soil maps for the most intensively used land in New Zealand and is being gradually extended to give national coverage. S-map provides data for extensively used soil models, such as the soil nutrient model OVERSEER and the daily simulation model APSIM used by agricultural scientists. McNeill et al. (2012) used the New Zealand National Soils Database to derive PTFs to estimate *θ(h)* at five tensions from morphological data of soils mapped in S-map. One of the current weaknesses of S-map is a lack of capacity to estimate *K(θ)*. Building on the work of Griffiths et al. (1999), Webb (2003) showed that morphologic descriptors for New Zealand soils can be used to predict K_s. However, the predictions of K_s were found to be too coarse for application to the wide range of soils within S-map. Therefore, Cichota et al. (2013) tested published statistical PTFs developed in Europe and the USA to predict *θ(h)* and *K(θ)* for a range of New Zealand soils. They combined the best two or three PTFs to construct ensemble PTFs. They considered the ensemble PTF for *θ(h)* to be a reasonable fit, but the ensemble PTF for estimating K_s exhibited large scatter and was not as reliable. The poor performance when estimating K_s was possibly due to the absence of any measurements of pore-size distribution in their physical predictors (Watt and Griffiths, 1988; McKenzie and Jacquier, 1997; Chapuis, 2004; Mbonimpa et al., 2002), and also to the large uncertainties in the measurements from small cores (McKenzie and Cresswell, 2002 ; Anderson and Bouma, 1973). Consequently, there is an urgent need in New Zealand to develop a physically based K_s model which is based on pore-size distribution.

Since PTFs developed to characterize *θ(h)* are more reliable than PTFs to characterize *K(θ)* (e.g., Balland and Pollacco, 2008; Cichota et al., 2013), Pollacco et al. (2013) developed a new physical model that predicts unimodal K_s solely from hydraulic parameters derived from the Kosugi (1996) *θ(h)*. The K_s model is derived by combining the Hagen-Poiseuille and Darcy law (Anon, 1993) and by incorporating three semi-empirical tortuosity parameters. The model is based on the soil pore-size distribution and has been successfully validated using the European HYPRES (Wösten et al., 1998; Wösten et al., 1999; Lilly et al., 2008) and the UNSODA databases (Leij et al., 1999; Schaap and van Genuchten, 2006), but has not yet been applied to New Zealand soils. Most New Zealand soils are considered to be structured, with two-stage drainage (Carrick et al., 2010; McLeod et al., 2008) and bimodal pore-size distribution (e.g. Durner, 1994). Romano and Nasta (2016) showed by using the HYDRUS-1D package that large errors arise in the computation of the water fluxes if unimodal *θ(h)* and *K(θ)* are used in structured soils. We therefore propose to improve the unimodal Pollacco et al. (2013) K_s model so that it can predict K_s for structured soils with bimodal porosity.

Measured K_s values are widely recognised as one of the most variable soil attributes (McKenzie and Cresswell 2002; Carrick, 2009). This is also recognised for New Zealand soils, both due to the high variability over short distances in soil parent material, age, depth and texture, as well as strong macropore development with preferential macropore flow recognised as the norm rather than the exception in New Zealand soils (Webb et al., 2000; Carrick, 2009; McLeod et al., 2008). The measurement variability is also expected to increase as the sampling diameter decreases because small cores provide an unrealistic representation of the abundance and connectivity of macropores (McKenzie and Cresswell, 2002; Anderson and Bouma, 1973). McKenzie and Cresswell (2002) suggest that the standard Australian laboratory measurements should use cores with minimum diameter of 25 cm and 20 cm length. In New Zealand, K_s has been obtained by using small cores, commonly with 10 cm diameter and 7.5 cm length. This has contributed to very high variability in measured K_s (Webb et al., 2000).

The objectives of this research were to:

- test the suitability of the unimodal Pollacco et al. (2013) K_s model to predict K_s from New Zealand soils,
- develop a K_s bimodal model that makes predictions in structured soils solely from hydraulic parameters derived from the Kosugi *θ(h)*,
- derive the uncertainties of the predictions of the K_s bimodal model,
- provide recommendations on the critical data sets that are required to improve the S-map database in New Zealand.

2 Background

2.1 Kosugi unimodal water retention and unsaturated hydraulic conductivity curve

There are a number of closed-form unimodal expressions in the literature that compute the soil moisture retention curve *θ(h)* and the unsaturated hydraulic conductivity *K(θ)* curves, such as the commonly used van Genuchten (1980) and Brooks and Corey (1964) curves. We selected the physically based Kosugi (1996) closed-form unimodal log-normal function expression of *θ(h)* and *K(θ)* because its parameters are theoretically sound and relate to the soil pore-size distribution (Hayashi et al., 2009). Soils have a large variation in pore radius, *r*, which follows a log-normal probability density function. The unimodal Kosugi log-normal probability density function of pore radius (*r*) is often written in the following form:

$$\frac{\mathrm{d}\theta}{\mathrm{d}r} = \frac{\theta_s - \theta_r}{r\,\sigma\,\sqrt{2\,\pi}}\exp\left\{-\frac{\left[\ln\left(r/r_m\right)\right]^2}{2\sigma^2}\right\} \tag{1}$$

where θ_r and θ_s [cm^3 cm^{-3}] are the *residual* and *saturated water contents*, r_m [cm] is the *median pore radius* and σ [-] denotes the *standard deviation* of ln(*r*).

Let S_e denote the effective saturation, defining $S_e(r) = (\theta - \theta_r)/(\theta_r - \theta_s)$, such that $0 \le S_e \le 1$. Integrating Eq. (1) from 0 to *r* yields the unimodal *water retention curve* as a function of *r*:

$$S_e(r) = \frac{1}{2} erfc\left[\frac{\ln\ r_m - \ln\ r}{\sigma\ \sqrt{2}}\right] \tag{2a}$$

$$\text{with}\quad r = \frac{r_m}{\exp\left[erfc^{-1}\left[2\ \ S_e\right]\sigma\sqrt{2}\right]} \tag{2b}$$

where *erfc* is the complementary error function.

The Young–Laplace capillary equation relates the soil-pore radius, r, to the equivalent *matric suction head*, h (cm), at which the pore is filled or drained (i.e., $r = Y/h$, where $Y = 0.149$ cm^2). Kosugi's unimodal *moisture retention curve* $\theta_{uni}(h)$ can be written in terms of S_e:

$$S_e(h) = \frac{1}{2} erfc\left[\frac{\ln h - \ln h_m}{\sigma\sqrt{2}}\right] \tag{3}$$

where h_m [cm] is the *median metric head*.

The unimodal Kosugi unsaturated hydraulic conductivity function $K(\theta)$ is written as:

$$K(S_e) = K_s \sqrt{S_e} \left\{\frac{1}{2} erfc\left[erfc^{-1}(2S_e) + \frac{\sigma}{\sqrt{2}}\right]\right\}^2 \tag{4}$$

where K_s (cm day^{-1}) is the *saturated hydraulic conductivity*.

θ_s is computed from the *total porosity*, ϕ, which is deduced from *bulk density* (ρ_b) and *soil particle density* (ρ_p) as follows:

$$\phi = \left[1 - \frac{\rho_b}{\rho_p}\right] \tag{5}$$

Due to air entrapment, θ_s seldom reaches saturation of the total pore space ϕ (Carrick et al., 2011). Therefore, to take into account the fact that not all pores are connected, we perform the following correction of ϕ with α in the range [0.9, 1]:

$$\theta_s = \alpha\,\phi \tag{6}$$

It is accepted that $\alpha = 0.95$ (Rogowski, 1971; Pollacco et al., 2013; Haverkamp et al., 2005; Leij et al., 2005), but in this study the optimal α was found to be 0.98, since using a value of 0.95 resulted in several soil samples with θ_5 (θ measured at 5 kPa) greater than θ_s, which is not physically plausible. This was due to the inaccuracy of measuring ϕ (discussed in Sect. 4.1).

The feasible range of the Kosugi hydraulic parameters is summarized in Table 1. The h_m and σ feasible range is taken from Pollacco et al. (2013), who combined data from the HYPRES (Wösten et al., 1998; Wösten et al., 1999; Lilly et al., 2008) and UNSODA (Leij et al., 1999; Schaap and van Genuchten, 2006) databases.

Table 1. please insert here

2.2 Pollacco unimodal saturated hydraulic conductivity model

The *saturated hydraulic conductivity* model, K_{s_uni} (Pollacco et al., 2013) computes K_s from the Kosugi parameters θ_s, θ_r, σ and h_m (or r_m). K_{s_uni} is based on the pore-size distribution (Eq. (1)) and the tortuosity of the pores. K_{s_uni} was derived by adopting the method of Childs and Collisgeorge (1950) and modelling the soil water flux through a continuous function of Kosugi (1996) pore-size distribution. This was performed by combining the Hagen-Poiseuille equation (Anon, 1993) with Darcy's law and introducing the connectivity and tortuosity parameters τ_1, τ_2 of Fatt and Dykstra (1951) and τ_3 of Vervoort and Cattle (2003). K_{s_uni} is computed as:

$$K_{s\_uni} = C\left(1-\tau_1\right)\,\left(\theta_s-\theta_r\right)^{\frac{1}{1-\tau_3}}\,\int_0^1 r^{2(1-\tau_2)}dS_e \tag{7}$$

with $C = \dfrac{1}{8}\dfrac{\rho_w\,g}{\eta}$

where for water at 20°C, density of water ρ_w = 0.998 g cm^{-3}, acceleration due to gravity g = 980.66 cm s^{-2}, dynamic viscosity of water η = 0.0102 g cm^{-1} s^{-1} and C is a constant equal to 1.03663 × 10^{9} cm day^{-1}.

Integrating with S_e instead of r avoids the complication of finding the minimum and maximum value of r. Isolating r of Eq. (2b) and replacing it in Eq. (7) gives:

$$K_{s\_uni}\left(S_e\right) = C\left(1-\tau_1\right)\,\left(\theta_s-\theta_r\right)^{\frac{1}{1-\tau_3}}\,\int_0^1 \left\{\frac{Y/h_m}{\exp\left[erfc^{-1}\left(2\,S_e\right)\sigma\sqrt{2}\right]}\right\}^{2(1-\tau_2)} dS_e \tag{8a}$$

or $$K_{s\_uni} = C\left(1-\tau_1\right)\,\left(\theta_s-\theta_r\right)^{\frac{1}{1-\tau_3}}\,\int_0^1 \left\{\frac{r_m}{\exp\left[erfc^{-1}\left(2\,S_e\right)\sigma\sqrt{2}\right]}\right\}^{2(1-\tau_2)} dS_e \tag{8b}$$

and $r_m = Y/\,h_m$ (Young–Laplace capillary equation)

where τ_1, τ_2, τ_3 are tortuosity parameters [0–1].

If tortuosity were not included (τ_1, τ_2, τ_3 = 0), the pore-size distribution model would mimic the permeability of a bundle of straight capillary tubes. Vervoort and Cattle (2003) state: "*In reality soils are much more complex, with twisted and crooked pores, dead-ending or connecting to other pores. This means that there is a need to scale the permeability from the capillary tube model to include increased path length due to crookedness of the path (tortuosity) or lack of connection between points in the soil (connectivity)*". Soils that are poorly connected and have highly crooked pathways theoretically have τ_1, τ_2, $\tau_3 \approx 0.9$. Further explanation of tortuosity is provided in Table 2.

Table 2. Please insert here

2.3. Romano bimodal water retention curve

New Zealand soils are predominantly well structured, with two-stage drainage (Carrick et al., 2010; McLeod et al., 2008), and therefore have a bimodal pore-size distribution (e.g. Durner, 1994). As K_{s_uni} is based on a unimodal curve, $\theta_{uni}(h)$, the proposed bimodal model, K_{s_bim}, should be based on a bimodal $\theta_{bim}(h)$ curve.

Borgesen et al. (2006) showed that structured soils have both *matrix* (inter-aggregate) pore spaces and *macropore* (intra-aggregate) pore spaces. Thus, when the pores are initially saturated ($r > R_{mac}$) or ($h < H_{mac}$), the flow is considered *macropore* flow, and when the soil is desaturated ($r < R_{mac}$) or ($h > H_{mac}$), the flow is considered *matrix flow*, as shown in Fig. 1. R_{mac} is the theoretical pore size r that delimits macropore and matrix flow and H_{mac} is the theoretical pressure that delimits macropore and matrix flow. To model bimodal pore-size distribution Durner (1994) superposes two unimodal pore-size distributions by using an empirical weighting factor, W, which partitions the volumetric percentage of macropore and matrix pores. Recently Romano et al. (2011) proposed the following Kosugi bimodal $\theta_{\mathrm{bim\_rom}}(h)$ distribution:

$$\theta_{bim\_\mathrm{rom}}(h) = (\theta_s - \theta_r)\left\{W\, erfc\left[\frac{\ln\, h - \ln\, h_{m\_mac}}{\sigma_{\_mac}\sqrt{2}}\right] + (1-W)\, erfc\left[\frac{\ln\, h - \ln\, h_m}{\sigma\,\sqrt{2}}\right]\right\} + \theta_r \tag{9}$$

where θ_{s}, $h_{\mathrm{m\_mac}}$ and $\sigma_{\_mac}$ are, respectively, the *saturated water content*, the *median pore radius* and the *standard deviation* of ln(h) of the macropore domain, θ_{r}, h_{m} and σ are parameters of the matrix domain, and W is a constant in the range [0,1).

3 Theoretical development of novel bimodal saturated hydraulic conductivity

We report on further adaptations to the physical model of Pollacco et al. (2013) to suit it to dual-porosity structured soils, which are common in New Zealand, solely from Kosugi hydraulic parameters describing $\theta(h)$. This involves:

- rewriting the Romano bimodal $\theta(h)$ (Sec. 3.1),
- developing a novel bimodal K_{s} model based on the modified bimodal $\theta(h)$ (Sec. 3.2).

3.1 Modified Romano bimodal water retention curve

We propose a modified version of $\theta_{\mathrm{bim\_rom}}(h)$ (Eq. (9)) that does not use the empirical parameter W. Our modified function, $\theta_{\mathrm{bim}}(h)$, is plotted in Fig. 1 and is computed as:

$$\theta_{bim}(h) = \theta_{bim\_mat}(h) + \theta_{bim\_mac}(h) \tag{10a}$$

$$\theta_{bim\_mat}(h) = \left[\theta_{s\_mac} - \theta_r\right]\, erfc\left[\frac{\ln\, h - \ln\, h_m}{\sigma\sqrt{2}}\right] + \theta_r \tag{10b}$$

$$\theta_{bim\_mac}(h) = \left[\theta_s - \theta_{s\_mac}\right]\, erfc\left[\frac{\ln\, h - \ln\, h_{m\_mac}}{\sigma_{\_mac}\sqrt{2}}\right] \tag{10c}$$

where $\theta_{\mathrm{s\_mac}}$ is the *saturated water content* that theoretically differentiates *macropore* and *matrix* domains.

The shape of $\theta_{\mathrm{bim}}(h)$ is identical to that of $\theta_{\mathrm{bim\_rom}}(h)$, but the advantage of $\theta_{\mathrm{bim}}(h)$ is that it uses the physical parameter $\theta_{\mathrm{s\_mac}}$ instead of the empirical parameter W, and $\theta_{\mathrm{s\_mac}}$ ($\leq\theta_{\mathrm{s}}$) is more easily parameterized than W particularly when there is no available data in the macropore domain. When we do not have data in the macropore domain, $\theta_{\mathrm{s\_mac}}$ is determined by fitting the hydraulic parameters $\theta_{\mathrm{s\_mac}}$, θ_{r}, h_{m}, σ of $\theta_{\mathrm{bim\_mat}}(h)$ (Eq. (10b)) solely in the matrix range ($r < R_{\mathrm{mac}}$ or h > H_{mac}) Fig. 1 shows that R_{mac} and $\theta_{\mathrm{s\_mac}}$ delimit the matrix and the macropore domains and that r_{m} of the Kosugi model is the inflection point of $\theta_{\mathrm{bim\_mat}}(h)$ and $r_{\mathrm{m\_mac}}$ is the inflection point of $\theta_{\mathrm{bim\_mac}}(h)$.

Fig. 1. Please put it here

3.2 Novel bimodal saturated hydraulic conductivity model

Using θ_{bim}(h), we propose a new bimodal K_{s_bim} that is derived following K_{s_uni} (Eq. (7)) but for which we add a macropore domain:

$$K_{s\_bim} = K_{s\_bim\_mat} + K_{s\_bim\_mac} \tag{11a}$$

$$K_{s\_bim\_mat} = C \int_0^1 \left(1-\tau_1\right) \left(\theta_{s\_mac} - \theta_r\right)^{\frac{1}{1-\tau_3}} \left(r_{matrix}\right)^{2(1-\tau_2)} \, dS_e \tag{11b}$$

$$K_{s\_bim\_mac} = C \int_0^1 \left(1-\tau_{1\_mac}\right) \left(\theta_s - \theta_{s\_mac}\right)^{\frac{1}{1-\tau_{3\_mac}}} \left(r_{macropore}\right)^{2\left(1-\tau_{2\_mac}\right)} dS_e \tag{11c}$$

where $r_{macropore}$ is $r \geq R_{mac}$ and r_{matrix} is $r < R_{mac}$.

The r_{matrix} of Eq. (11b) is derived from Eq. (2b):

$$r_{matrix} = \frac{r_m}{\exp\left[erfc^{-1}\left[2 \;\, S_e\right] \sigma \sqrt{2}\right]} \tag{12}$$

and $r_{macropore}$ is computed similarly as:

$$r_{macropore} = \frac{r_{m\_mac}}{\exp\left[erfc^{-1}\left[2 \;\, S_e\right] \sigma_{\_mac} \sqrt{2}\right]} \tag{13}$$

We introduced r_{matrix} (Eq. (12)) and $r_{macropore}$ (Eq. (13)) into K_{s_bim} (Eq. (11a)), giving the equation for K_{s_bim}:

$$K_{s\_bim} = C \int_0^1 \left[\begin{array}{l} \left(1-\tau_1\right) \left(\theta_{s\_mac} - \theta_r\right)^{\frac{1}{1-\tau_3}} \left\{ \dfrac{r_m}{\exp\left[erfc^{-1}\left[2 \;\, S_e\right] \sigma \sqrt{2}\right]} \right\}^{2(1-\tau_2)} + \\ \left(1-\tau_{1_{\_mac}}\right) \left(\theta_s - \theta_{s\_mac}\right)^{\frac{1}{1-\tau_{3\_mac}}} \left\{ \dfrac{r_{m\_mac}}{\exp\left[erfc^{-1}\left[2 \;\, S_e\right] \sigma_{\_mac} \sqrt{2}\right]} \right\}^{2\left(1-\tau_{2\_mac}\right)} \end{array} \right] dS_e \tag{14a}$$

or

$$K_{s\_bim} = C \int_0^1 \left[\begin{array}{l} \left(1-\tau_1\right) \left(\theta_{s\_mac} - \theta_r\right)^{\frac{1}{1-\tau_3}} \left\{ \dfrac{\dfrac{Y}{h_m}}{\exp\left[erfc^{-1}\left(2\, S_e\right) \sigma \;\sqrt{2}\right]} \right\}^{2(1-\tau_2)} + \\ \left(1-\tau_{1_{\_mac}}\right) \left(\theta_s - \theta_{s\_mac}\right)^{\frac{1}{1-\tau_{3\_mac}}} \left\{ \dfrac{\dfrac{Y}{h_{m\_mac}}}{\exp\left[erfc^{-1}\left(2\, S_e\right) \sigma_{\_mac} \sqrt{2}\right]} \right\}^{2(1-\tau_{2\_mac})} \end{array} \right] dS_e \tag{14b}$$

In Eq. (14b), r_{m_mac} is replaced by Y/h_{m_mac} and r_m is replaced by $Y/\, h_m$. Note that the bimodal K_s model requires that the flow in the macropore domain obeys the Buckingham–Darcy law. Therefore, this model's performance may be restricted in cases of non-Darcy flow, such as non-laminar and turbulent flow, which may occur in large macropores.

In this study $\sigma_{\_mac}$ is not derived from measured $\theta(h)$ because measured data in the macropore domain are not always available, and so it will be treated as a fitting parameter. As discussed above, θ_{s_mac}, θ_r, σ and h_m are optimized with $\theta_{uni}(h)$ measurement points only in the matrix range ($r < R_{mac}$ or h > H_{mac}), which means that θ_s is not included in the observation data. In summary, K_{s_bim} requires optimization of the parameters τ_1, τ_2, τ_3, and τ_{1_mac}, τ_{2_mac}, τ_{3_mac} and h_{m_mac}, $\sigma_{\_mac}$ (if no data are available in the macropore domain). The theoretically feasible range of the parameters of K_{s_bim} is shown in Table 3.

Table 3. Please put table here.

One of the limitations of the New Zealand data set is that it has no $\theta(h)$ data points in the macropore domain. The closest data point near saturation is $\theta(h = 50\text{ cm})$, which is in the matrix pore space. Carrick et al. (2010) found that H_{mac} ranges from 5 to 15 cm, with an average H_{mac} = 10 cm, which corresponds to a circular pore radius of R_{mac} = 0.0149 cm (e.g. Jarvis, 2007; Jarvis and Messing, 1995; Messing and Jarvis, 1993). Therefore, to reduce the number of optimized parameters we make the following assumption:

$$h_{m\_mac} = \exp\left[\frac{\ln(H_{mac})}{P_{m\_mac}}\right] \tag{15}$$

where P_{m_mac} is a fitting parameter greater than 1. We found the fitted value of P_{m_mac} was 2.0, however this fitted parameter was very broadly determined. The cause might be that we are optimizing $\sigma_{\_mac}$ and therefore h_{m_mac} and $\sigma_{\_mac}$ might be *linked*. *Linked parameters* (Pollacco et al., 2008a, 2008b, 2009) means that there is an infinite combination of sets of linked parameters h_{m_mac} and $\sigma_{\_mac}$ which produces values of objective function close to that obtained with the optimal parameter set and for which there exists a continuous relationship between h_{m_mac} and $\sigma_{\_mac}$. Further research needs to determine if having more data in the macropore domain would reduce the cause of non-uniqueness. To illustrate h_{m_mac}, the equivalent r_{m_mac} point is shown in Fig. 1, where r_{m_mac} is the inflection point of the macropore domain. Fig. 1 also shows that the matrix and the macropore domains meet at R_{mac} (H_{mac}).

4 Methods

4.1 Measurement of physical soil properties

The soil data used in this study were sourced from two data sets. In the first data set (Canterbury Regional Study; Table 4) soils were derived from eight soils series on the post-glacial and glacial alluvial fan surfaces of the Canterbury Plains (Webb et al., 2000). The soils varied from shallow, well-drained silt loam soils to deep, poorly drained clay loam soils. The second data set was derived from the Soil Water Assessment and Measurement Programme to physically characterize key soils throughout New Zealand in the 1980s. Soils selected from this data set are listed by region in Table 4 and were selected from soils formed from sediments derived from indurated sandstone rocks, because this is the most common parent material for soils in New Zealand and has a reasonably representative number of soils analysed for physical properties.

The cores for particle size analysis and measurement of $\theta(h)$ had diameters which ranges from 5.5 cm to 10 cm diameter and having height which varied from 5 to 6 cm. The 5, 10 kPa measurements of the $\theta(h)$ were derived using the suction table method as per Dane and Topp, (2002) following the NZ Soil Bureau laboratory method (Gradwell, 1972). For the 20 to 1500 kPa of the $\theta(h)$ were measured using pressure plate method as per Dane and Topp, (2002), following the NZ Soil Bureau method (Gradwell, 1972). The laboratory analysis for particle size followed Gradwell (1972).

The total porosity, ϕ, described in Eq. (5) contains uncertainties from the measurement methods, where ϕ is derived from separate measurements of particle density and bulk density, rather than being directly measured. The uncertainty in ϕ measurements appeared to have reduced the demonstrated benefits of using K_{s_bim} instead of K_{s_uni}, which strongly relies on $\phi\ \alpha - \theta_{s\_mac}$ and may have caused the optimal α to be 0.98 and not the commonly accepted value of 0.95 (Rogowski, 1971; Pollacco et al., 2013; Haverkamp et al., 2005; Leij et al., 2005).

Table 4. Please put here

The K_s data used were collected and processed at a time when the best field practices in New Zealand were still being explored. K_s was derived using constant-head Mariotte devices (1 cm head) from three to six cores (10 cm diameter and 7.5 cm thickness) for each horizon. The $\log_{10}$ scale value of the standard error of the replicates of the measurements is shown in Fig. 2, which shows large uncertainty in the measurements (up to three orders of magnitude). This uncertainty is due to:

a) **measurements of $\theta(h)$ and K_s being taken on different cores**, which caused some mismatch between $\theta(h)$ and K_s, resulting in 16 outliers that negatively influenced the overall fit of the K_s model having to be removed from the data set,

b) **side leakage** of some cores, which led to K_s values that were too high (Carrick, 2009), resulting in six samples with unusually high K_s having to be removed from the data set,

c) **misreporting low K_s** since the measurements of K_s were halted when conductivity was less than 0.1 cm day^{-1}, resulting in four samples with low K_s having to be removed from the data set,

d) **small core samples,** which led to considerable variability in the absence/presence of structured cracks caused by roots or worm burrows (McKenzie and Cresswell, 2002; Anderson and Bouma, 1973) that were evident in dyed samples; we therefore removed measured K_s replicates that were too high and showed evidence of macropore abundance by having values of $\theta_s - \theta_{s\_mac} > 0.05$.

We therefore selected 235/262 samples (90%) and removed only 27 outliers, which is minimal compared, for instance, to the UNSODA (Leij et al., 1999; Schaap and van Genuchten, 2006) and HYPRES databases (Wösten et al., 1998; Wösten et al., 1999; Lilly et al., 2008), which are used for the development of PTFs such as the ROSETTA PTF (Patil and Rajput, 2009; Rubio, 2008; Young, 2009), and which were found to contain a large number of outliers. Using these databases, Pollacco et al. (2013) selected only 73/318 soils (23%), which complied with strict selection criteria prior to modelling.

Note that the K_s observations in the topsoils have greater variability than in the subsoil layers (Fig. 2). This is because topsoils are more disturbed by anthropogenic disturbance and biological activity. Therefore, the topsoils also have a greater abundance of macropores, and therefore are more prone to error when the sampling is performed with a small core size that does not contain a representative volume of the macropore network.

Fig. 2. Please insert figure here

4.2 Inverse modelling and goodness of fit

The parameterization of the model was performed in two consecutive steps:

1. Optimization of θ_{s_mac}, θ_r, h_m and σ of the unimodal Kosugi $\theta_{bim\_mat}(h)$ (Eq. (10b)) was performed by matching observed and simulated $\theta(h)$ in the range $h < H_{mac}$ (as discussed, θ_s is not included in the observation data since we did not have data in the macropore domain). The feasible ranges of the Kosugi parameters are described in Table 1.
2. Optimization of the τ_1, τ_2, τ_3 of the K_{s_uni} model (Eq. (8)) and τ_{1_mac}, τ_{2_mac}, τ_{3_mac}, $\sigma_{\_mac}$ parameters of the K_{s_bim} models (Eq. (14)), where the physical feasible ranges of the tortuosity parameters are described in Table 3.

The inverse modelling was performed in MATLAB using AMALGAM, which is a robust global optimization algorithm (http://faculty.sites.uci.edu/jasper/sample/) (e.g., ter Braak and Vrugt, 2008). For each step, we minimized the objective functions described below.

The objective function, OF_θ, used to parameterize Kosugi's $\theta(h)$ at the following pressure points [5, 10, 20, 40, 50, 100, 1500 kPa], is described by:

$$OF_\theta = \sum_{i=1}^{i=N_\theta} \left[\theta_{sim}\left(h_i, \mathbf{p}_\theta\right) - \theta_{obs}\left(h_i\right)\right]^{P_{ower}} \tag{16}$$

where the subscripts *sim* and *obs* are simulated and observed, respectively. P_θ is the set of predicted parameters (θ_{s_mac}, θ_r, h_m, σ) and P_{ower} is the power of the objective function. The computation of K_{s_bim} requires $\theta(h)$ to be accurate near saturation, when the drainage is mostly from large pores, and to achieve this balance we found by trial and error that best results are achieved when $P_{ower} = 6$.

The parameters of K_{s_uni} and K_{s_bim} models were optimized by minimizing the following objective function OF_{ks}:

$$OF_{ks} = \sum_{j=1}^{j=N_{ks}} \left[\ln K_{s\_sim}\left(\mathbf{p_{ks}}\right) - \ln K_{s\_obs}\right]^2 \tag{17}$$

where the subscripts *sim* and *obs* are simulated and observed, respectively. P_{ks} is the vector of the unknown parameters. The log transformation of OF_{ks} puts more emphasis on the lower K_s and therefore reduces the bias towards larger conductivity (e.g. van Genuchten et al., 1991; Pollacco et al., 2011). Also, the log transformation considers that the uncertainty in measured unsaturated hydraulic conductivity increases as $K(\theta)$ increases.

The goodness of fit between simulated (K_{s_uni} or K_{s_bim}) and observed K_s was computed by the $RMSE_{log10}$:

$$RMSE_{\log 10} = \sqrt{\frac{\sum_{j=1}^{j=N_{ks}} \left[\log_{10} K_{s\_sim} - \log_{10} K_{s\_obs}\right]^2}{N}} \tag{18}$$

where N is the number of data points.

The following transformation was necessary to scale the parameters to enable the global optimization to converge to a solution:

$$\tau_1 = 1 - 10^{-T1} \tag{19}$$

where T_1 is a transformed tortuosity τ_1. Introducing Eq. (19) into K_{s_bim} Eq. (14) gives:

$$K_{s\_bim} = C \int_0^1 \left[\begin{array}{l} 10^{-T_1} \left(\theta_{s\_mac} - \theta_r\right)^{\frac{1}{1-\tau_3}} \left\{ \dfrac{\dfrac{Y}{h_m}}{\exp\left[erfc^{-1}\left(2\, S_e\right) \sigma \, \sqrt{2} \right]} \right\}^{2(1-\tau_2)} + \\ 10^{-T_{1\_mac}} \left(\theta_s - \theta_{s\_mac}\right)^{\frac{1}{1-\tau_{3\_mac}}} \left\{ \dfrac{\dfrac{Y}{h_{m\_mac}}}{\exp\left[erfc^{-1}\left(2\, S_e\right) \sigma_{\_mac} \sqrt{2} \right]} \right\}^{2(1-\tau_{2\_mac})} \end{array} \right] dS_e \qquad (20)$$

5 Results and discussion

We report on (1) the suitability of the K_{s_uni} model (developed with European and American data sets, Pollacco et al., 2013) to predict K_s for New Zealand soils experiencing large uncertainties, as shown in Fig. 2; (2) improvements made by stratifying the data with texture and topsoil/subsoil; and (3) enhancements made by using the bimodal K_{s_bim} instead of the unimodal K_{s_uni}.

5.1 Improvement made by stratifying with texture and topsoil/subsoil

It was expected that stratifying with texture and topsoil/subsoil (layers) should improve the predictions of K_s to only a modest degree. This is because K_{s_bim} and K_{s_uni} are physically based models that are based on pore-size distribution, and therefore stratifying with soil texture or topsoil/subsoil are not likely to provide extra information. For instance, Arya and Paris (1981) showed that there is a strong relationship between pore-size distribution and the particle-size distribution and therefore adding soil texture information should not improve the model.

Table 5. please put table here

As expected, no significant improvements were made by stratifying with soil texture compared with a model that groups all texture classes (loam and clay) and layers (topsoil and subsoil) (overall improvement of 3%) (Table 5). However, a significant improvement was made by stratifying by layer (topsoil and subsoil) (overall improvement of 23%), and therefore the remaining results are presented by stratifying by layer. These results are obtained because topsoils have higher macropores and a smaller tortuous path than that in subsoil, as demonstrated by $\tau_{1\_top} > \tau_{1\_sub}$ or $T_{1\_top} < T_{1\_sub}$, $\tau_{2\_top} > \tau_{2\_sub}$, $\tau_{3\_top} > \tau_{3\_sub}$ (Table 6). It is important to note that tortuosity decreases as τ becomes closer to 1.

Table 6. Please put table here

5.2 Improvement made by using K_{s_bim} instead of K_{s_uni}

Figure 3 shows an acceptable fit between K_{s_bim} and K_{s_obs} (RMSElog$_{10}$ = 0.450 cm day^{-1}), recognizing that the observations contain large uncertainties since the measurements were taken by using small cores (Sect. 4.1). The overall improvement made by using K_{s_bim} is somewhat modest (5% for all soils). As expected, the reasonable improvement is greater for topsoil containing higher macroporosity (12% improvement) than for subsoil (4% improvement) (Table 6). This is because topsoil has higher macropore θ_{mac} (θ_s–θ_{s_mac}) (Table 7) caused by earthworm channels, fissures, roots and tillage than subsoil. The RMSElog$_{10}$ of K_{s_uni} for subsoil is 0.47 cm day^{-1} (Table 6) which is slightly worse compared to the RMSElog$_{10}$ of 0.420 cm day^{-1} by using UNSODA and HYPRES data sets (Pollacco et al., 2013).

Table 7. Please put table here

The reason K_{s_bim} shows smaller-than-expected improvements compared to K_{s_uni} requires further investigation and testing with a data set containing fewer uncertainties. One plausible explanation is that K_{s_bim} is highly sensitive to θ_s, computed from total porosity ϕ (Eq. (6)), which had inherent measurement uncertainties (Sect. 4.1). In addition, the possible existence of non-Darcy flow in large biological pores may decrease the outperformance of the bimodal model over the unimodal model.

Fig. 3. Please insert Figure 3 here

5.3 Optimal tortuosity parameters

The optimal tortuosity parameters of K_{s_bim} and K_{s_uni} (Table 6) show that the optimal parameters are within the physically feasible limits, except for τ_{3_mac} of the subsoil, which are greater than τ_3. This is understandable because Pollacco et al. (2013) found τ_3 not to be a very sensitive parameter. As expected, T_{1_mac} is smaller than T_1 ($\tau_{1\_mac} > \tau_1$), which suggests that the tortuosity parameters have a physical meaning.

The estimated value of the unimodal T_1 parameter K_{s_uni} derived from the UNSODA and HYPRES data sets (T_1 = 0.1) (Pollacco et al., 2013) is very different from the value estimated in this present study (T_1 = 6.5). Cichota et al. (2013) also reported that PTFs developed in Europe and the USA were not applicable to New Zealand. The reasons why these PTFs are not directly applicable to New Zealand require further investigation.

5.4 Uncertainty of the bimodal saturated hydraulic conductivity model predictions

The practical application of the bimodal saturated hydraulic conductivity model, K_{s_bim}, to New Zealand soils requires a model for the uncertainty of the resultant predictions, since it is then possible to attach a value for the uncertainty of future predictions of K_s. In a conventional parametric statistical model, the uncertainty model follows from the structure of the fitting model itself. In the present work, K_s is estimated using an inverse model and this has no associated functional uncertainty model. For this reason, the uncertainty is derived empirically by fitting a relationship between the transformed residuals of the model (the log-transformed measured K_s minus the log-transformed estimated K_s) as a function of the log-transformed estimated K_s. Although the uncertainty model could be derived from all the soils in the study, this process results in a pooled estimate for uncertainty (e.g., aggregated root mean square error). However, it has been observed that topsoils and subsoils have different uncertainty behaviour for the estimated K_s, so it is desirable to include an indicator variable to determine whether the soil is a topsoil or not. In explicit form,

$$\log_{10} K_{s\ obs} - \log_{10} K_{s\ sim} = a_1 L + a_0 + \epsilon \qquad (21)$$

where a_0 and a_1 are fitting constants, L is an indicator variable specifying whether the soil is a topsoil (value 1), or a subsoil (value 0), and ϵ is the uncertainty distribution. The distribution of the uncertainty ϵ could take a number of forms, but there is no obvious choice, except that one might expect the distribution central measure to be unbiased. To avoid an explicit distribution assumption, we fitted a conditional quantile model (Koenker, 2005) for the transformed residuals, based on the τ quantile, where $\tau = 0.5$ corresponds to the conditional median, and $\tau = 0.025$ and $\tau = 0.975$ correspond respectively to the 2.5% and 97.5% quantiles, and thus together describe the 95% containment interval of the residuals.

The conditional quantile model Eq. (21) was fitted using $\tau = 0.5, 0.025$ and 0.975 (Table 8). The results suggest a strong dependence of the scale of the residuals on whether the soil is a topsoil or not, but the size of the 95% residual containment interval is not dependent on the simulated K_s. Notably, the confidence interval for the fitted median ($\tau = 0.5$) quantile model suggests that the uncertainty distribution median is unbiased; thus predictions from K_{s_bim} show no propensity for bias, which is a desirable result.

Table 8. Please put here

Another way to illustrate the uncertainty model is to plot the observed $\log_{10} K_{s\_obs}$ against the estimated $\log K_{s\_bim}$, with the fitted median, lower and upper 95% quantile lines, as shown in Fig. 4. The width of the 95% containment interval for the residuals is narrower (i.e., the predictions appear to be more accurate) for topsoils. The quantile estimates for the conditional median of both topsoil and subsoil are also shown in Fig. 4, with the shaded region showing the 95% confidence interval of the median estimate. The shaded region covers the one-to-one line in Fig. 4, and thus there is no compelling evidence that the median residual distribution is biased.

Fig. 4. Please put here

6 Recommended future work to improve the New Zealand soil database

A key outcome of this research will be to provide direction for future field studies to quantify soil water movement attributes of New Zealand soils, and to prioritise which measurements will have the greatest value to reduce the uncertainty in modelling of the soil moisture retention and hydraulic conductivity relationships. Recommendations are:

- Evaluate the spatial representativeness of the current soil physics data set and undertake more measurements of hydraulic conductivity and soil water retention on key soils,
- Use larger cores for measurements of hydraulic conductivity,
- Take measurements of the moisture retention curve and saturated hydraulic conductivity on the same sample,
- Provide more accurate measurements of total porosity.

- Conduct near saturation measurements of $\theta(h)$ and $K(\theta)$ to better characterize the macropore domain, which is responsible for preferential flow behaviour,
- Make more accurate measurements on slowly permeable soils (< 1 cm day^{-1}), which are important for management purposes but are not well represented in the current databases.

7 Conclusions

We report here on further adaptations to the saturated hydraulic conductivity unimodel to suit it to dual-porosity structured soils by computing the soil water flux through a continuous function of a modified version of Romano et al. (2011) $\theta(h)$ dual pore-size distribution. The shape of the Romano $\theta(h)$ distribution is identical to the modified $\theta(h)$, but the advantage of the developed bimodal $\theta(h)$ is that it is more easily parameterized when no data are available in the macropore domain.

The stratification of the data with texture only (loam or clay) slightly improved the predictions of the K_s model, which is based on pore-size distribution. This gives us confidence that the K_s model is accounting for the effect of these physical parameters on K_s. A significant improvement was made by separating topsoils from subsoils. The improvements are higher for the topsoil, which has higher macroporosity caused by roots and tillage compared to subsoils. The reason why a model with no stratification is not sufficient is unclear and requires further investigation.

The improvements made by using the developed bimodal K_{s_bim} (Eq. 20) compared to the unimodal K_{s_uni} (Eq. 8) is modest overall, but, as expected, greater for topsoils having larger macroporosity. Nevertheless, an acceptable fit between K_{s_bim} with K_{s_obs} was obtained when due recognition was given to the high variability in the measured data. We expect K_{s_bim} to provide greater improvement in K_s predictions if more $\theta(h)$ measurements are made at tensions near saturation and if measurements are made on larger cores and with more accurate measurements of porosity.

Data availability

The data are part of the New Zealand soil databases, available at http://smap.landcareresearch.co.nz/ and https://soils.landcareresearch.co.nz/.

Acknowledgements

We are grateful to Leah Kearns and for Ray Prebble, who improved the readability of the manuscript and for anonymous reviewers who significantly improved the clarity of the manuscript. We are also thankful for Dr Ian Lynn for his input on soil heterogeneity. This project was funded by Landcare Research core funding, through the New Zealand Ministry of Business, Innovation and Employment.

References

Anon: The History of Poiseuille's Law, Annual Review of Fluid Mechanics, 25(1), 1–20, doi:10.1146/annurev.fl.25.010193.000245, 1993.

Anderson, J. L., and Bouma, J.: Relationships between saturated hydraulic conductivity and morphometric data of an argillic horizon1, Soil Sci. Soc. Am. J., 37, 408-413, doi:10.2136/sssaj1973.03615995003700030029x, 1973b.

Arya, L. M., and Paris, J. F.: A physicoempirical model to predict the soil moisture characteristic from particle-size distribution and bulk density data, Soil Science Society of America Journal, 45, 1023–1030, doi:10.2136/sssaj1981.03615995004500060004x, 1981.

Balland, V., and Pollacco, J. A. P.: Modeling soil hydraulic properties for a wide range of soil conditions, Ecological Modelling, 219, 300–316, 2008.

Borgesen, C. D., Jacobsen, O. H., Hansen, S., and Schaap, M. G.: Soil hydraulic properties near saturation, an improved conductivity model, Journal of Hydrology, 324, 40–50, doi:10.1016/j.jhydrol.2005.09.014, 2006.

Brooks, R. H., and Corey, A. T.: Hydraulic properties of porous media, Hydrol. Pap., 3, 1964.

Carrick, S.: The dynamic interplay of mechanisms governing infiltration into structured and layered soil columns, PhD, Lincoln University, Lincoln, 2009.

Carrick, S., Almond, P., Buchan, G., and Smith, N.: In situ characterization of hydraulic conductivities of individual soil profile layers during infiltration over long time periods, European Journal of Soil Science, 61, 1056–1069, doi:10.1111/j.1365-2389.2010.01271.x, 2010.

Carrick, S., Buchan, G., Almond, P., and Smith, N.: Atypical early-time infiltration into a structured soil near field capacity: the dynamic interplay between sorptivity, hydrophobicity, and air encapsulation, Geoderma, 160(3–4), 579–589, doi:10.1016/j.geoderma.2010.11.006, 2011.

Chapuis, R. P.: Predicting the saturated hydraulic conductivity of sand and gravel using effective diameter and void ratio, Can. Geotech. J., 41(5), 787–795, doi:10.1139/t04-022, 2004.

Childs, E. C., and Collisgeorge, N.: The permeability of porous materials, Proc. R. Soc. Lon. Ser-A, 201, 392-405, doi:10.1098/rspa.1950.0068, 1950.

Cichota, R., Vogeler, I., Snow, V. O., and Webb, T. H.: Ensemble pedotransfer functions to derive hydraulic properties for New Zealand soils, Soil Research, 51, 94–111, doi:10.1071/sr12338, 2013.

Dane, J.H., and Topp, G. C.: Methods of Soil Analysis, Part 4. Physical Methods. Soil Science Society of America Book Series No. 5. Madison, WI, USA Pages 692-698, 2002

Durner, W.: Hydraulic conductivity estimation for soils with heterogeneous pore structure, Water Resources Research, 30, 211–223, doi:10.1029/93wr02676, 1994.

Fatt, I., and Dykstra, H.: Relative permeability studies, T. Am. I. Min. Met. Eng., 192, 249–256, 1951.

Gradwell, M. W.: Methods for physical analysis of soils. In New Zealand Soil Bureau Scientific Report No. 10C, 1972.

Griffiths, E., Webb, T. H., Watt, J. P. C., and Singleton, P. L.: Development of soil morphological descriptors to improve field estimation of hydraulic conductivity, Australian Journal of Soil Research, 37, 971–982, doi:10.1071/sr98066, 1999.

Haverkamp, R., Leij, F. J., Fuentes, C., Sciortino, A., and Ross, P. J.: Soil water retention: I. Introduction of a shape index, Soil Science Society of America Journal, 69, 1881–1890, doi:10.2136/sssaj2004.0225, 2005.

Hayashi, Y., Kosugi, K., and Mizuyama, T.: Soil water retention curves characterization of a natural forested hillslope using a scaling technique based on a lognormal pore-size distribution, Soil Science Society of America Journal, 73, 55–64, 2009.

Jarvis, N. J., and Messing, I.: Near-saturated hydraulic conductivity in soils of contrasting texture measured by tension infiltrometers, Soil Science Society of America Journal, 59, 27–34, 1995.

Jarvis, N. J.: A review of non-equilibrium water flow and solute transport in soil macropores: principles, controlling factors and consequences for water quality, European Journal of Soil Science, 58, 523–546, doi:10.1111/j.1365-2389.2007.00915.x, 2007.

Koenker, R.: Quantile Regression, Cambridge University Press, New York, 2005.

Kosugi, K.: Lognormal distribution model for unsaturated soil hydraulic properties, Water Resources Research, 32, 2697–2703, doi:10.1029/96wr01776, 1996.

Landcare Research, S-map - New Zealand's national soil layer: http://smap.landcareresearch.co.nz, 2015.

Leij, F. J., Alves, W. J., van Genuchten, M. T., and Williams, J. R.: The UNSODA unsaturated soil hydraulic database, in: Proceedings of the International Workshop on Characterization and Measurement of the Hydraulic Properties of Unsaturated Porous Media, 1269–1281, 1999.

Leij, F. J., Haverkamp, R., Fuentes, C., Zatarain, F., and Ross, P. J.: Soil water retention: II. Derivation and application of shape index, Soil Science Society of America Journal, 69, 1891–1901, doi:10.2136/sssaj2004.0226, 2005.

Lilburne, L. R., Hewitt, A. E., and Webb, T. W.: Soil and informatics science combine to develop S-map: a new generation soil information system for New Zealand, Geoderma, 170, 232–238, doi:10.1016/j.geoderma.2011.11.012, 2012.

Lilly, A., Nemes, A., Rawls, W. J., and Pachepsky, Y. A.: Probabilistic approach to the identification of input variables to estimate hydraulic conductivity, Soil Science Society of America Journal, 72, 16–24, doi:10.2136/sssaj2006.0391, 2008.

Mbonimpa, M., Aubertin, M., Chapuis, R. P. and Bussière, B.: Practical pedotransfer functions for estimating the saturated hydraulic conductivity, Geotechnical and Geological Engineering, 20(3), 235–259, doi:10.1023/A:1016046214724, 2002.

McKenzie, N., and Jacquier, D.: Improving the field estimation of saturated hydraulic conductivity in soil survey, Australian Journal of Soil Research, 35, 803–825, doi:10.1071/s96093, 1997.

McKenzie, N. J., and Cresswell, H. P.: Field sampling. In: Soil Physical Measurement and Interpretation for Land Evaluation, CSIRO, Collingwood, Victoria, 2002

McLeod, M., Aislabie, J., Ryburn, J., and McGill, A.: Regionalizing potential for microbial bypass flow through New Zealand soils, Journal of Environmental Quality, 37, 1959–1967, doi:10.2134/jeq2007.0572, 2008.

McNeill, S., Webb, T., and Lilburne, L.: Analysis of soil hydrological properties using S-map data., Landcare Research report 977, 2012.

Messing, I., and Jarvis, N. J.: Temporal variation in the hydraulic conductivity of a tilled clay soil as measured by tension infiltrometers, Journal of Soil Science, 44, 11–24, 1993.

Patil, N. G., and Rajput, G. S.: Evaluation of water retention functions and computer program "ROSETTA" in predicting soil water characteristics of seasonally impounded shrink-swell soils, Journal of Irrigation and Drainage Engineering-ASCE, 135, 286–294, doi:10.1061/(asce)ir.1943-4774.0000007, 2009.

Pollacco, J. A. P.: A generally applicable pedotransfer function that estimates field capacity and permanent wilting point from soil texture and bulk density, Canadian Journal of Soil Science, 88, 761–774, 2008.

Pollacco, J. A. P. and Angulo-Jaramillo, R.: A Linking Test that investigates the feasibility of inverse modelling: Application to a simple rainfall interception model for Mt. Gambier, southeast South Australia, Hydrological Processes, 23(14), 2023–2032

Pollacco, J. A. P., Braud, I., Angulo-Jaramillo, R. and Saugier, B.: A Linking Test that establishes if groundwater recharge can be determined by optimising vegetation parameters against soil moisture, Annals of Forest Science, 65(7)

Pollacco, J. A. P., Ugalde, J. M. S., Angulo-Jaramillo, R., Braud, I. and Saugier, B.: A Linking Test to reduce the number of hydraulic parameters necessary to simulate groundwater recharge in unsaturated soils, Adv Water Resour, 31(2), 355–369, doi:10.1016/j.advwatres.2007.09.002, 2008b.

Pollacco, J. A. P., Nasta, P., Ugalde, J. M. S., Angulo-Jaramillo, R., Lassabatere, L., Mohanty, B. P., and Romano, N.: Reduction of feasible parameter space of the inverted soil hydraulic parameters sets for Kosugi model, Soil Science, SS-S-12-00268, 2013.

Romano, N. and Nasta, P.: How effective is bimodal soil hydraulic characterization? Functional evaluations for predictions of soil water balance, Eur. J. Soil Sci., 67(4), 523–535, doi:10.1111/ejss.12354, 2016.

Romano, N., Nasta, P., Severino, G. and Hopmans, J. W.: Using Bimodal Lognormal Functions to Describe Soil Hydraulic Properties, Soil Sci. Soc. Am. J., 75(2), 468–480, doi:10.2136/sssaj2010.0084, 2011.

Rogowski, A. S.: Watershed physics – model of soil moisture characteristic, Water Resources Research, 7, 1575–1582, 1971 doi:10.1029/WR007i006p01575, 1971.

Rubio, C. M.: Applicability of site-specific pedotransfer functions and ROSETTA model for the estimation of dynamic soil hydraulic properties under different vegetation covers, Journal of Soils and Sediments, 8, 137–145, doi:10.1065/jss2008.03.281, 2008.

Schaap, M. G., and van Genuchten, M. T.: A modified Mualem-van Genuchten formulation for improved description of the hydraulic conductivity near saturation, Vadose Zone Journal, 5, 27–34, 2006.

ter Braak, C. J. F., and Vrugt, J. A.: Differential evolution Markov chain with snooker updater and fewer chains, Statistics and Computing, 4, 435–446, 2008.

van Genuchten, M. T.: Closed-form equation for predicting the hydraulic conductivity of unsaturated soils, Soil Science Society of America Journal, 44, 892–898, 1980.

van Genuchten, M. T., Leij, F. J., and Yates, S. R.: The RETC code for quantifying the hydraulic functions of unsaturated soils, The RETC Code for Quantifying the Hydraulic Functions of Unsaturated Soils, U.S. Department of Agriculture, Agricultural Research Service 1991.

Vervoort, R. W., and Cattle, S. R.: Linking hydraulic conductivity and tortuosity parameters to pore space geometry and pore-size distribution, Journal of Hydrology, 272, 36–49, 2003.

Watt, J. P. C., and Griffiths, E.: Correlation of hydraulic conductivity measurements with other physical properties New Zealand, New-Zealand Soil Bureau Commentaries, 1983, 198–201, 1988.

Webb, T. H., Claydon, J. J., and Harris, S. R.: Quantifying variability of soil physical properties within soil series to address modern land-use issues on the Canterbury plains, New Zealand, Australian Journal of Soil Research, 38, 1115–1129, doi:10.1071/sr99091, 2000.

Webb, T. H., Claydon, J. J. and Harris, S. R.: Quantifying variability of soil physical properties within soil series to address modern land-use issues on the Canterbury Plains, New Zealand Soil Res., 38(6), 1115–1129, doi:10.1071/SR99091, , 2000.

Webb, T. H.: Identification of functional horizons to predict physical properties for soils from alluvium in Canterbury, New Zealand, Australian Journal of Soil Research, 41, 1005–1019, doi:10.1071/sr01077, 2003.

Wösten, J. H. M., Lilly, A., Nemes, A., and Le Bas, C.: Final report on the EU funded project using existing soil data to derive hydraulic parameters for simulation models in environmental studies and in land use planning, DLO Winand Staring Centre, Wageningen,The Netherlands, 1998.

Wösten, J. H. M., Lilly, A., Nemes, A., and Le Bas, C.: Development and use of a database of hydraulic properties of European soils, Geoderma, 90, 169–185, 1999.

Young, C. D.: Overview of ROSETTA for estimation of soil hydraulic parameters using support vector machines, Korean Journal of Soil Science & Fertilizer, 42, 18–23, 2009.

Tables

Table 1. Feasible range of the Kosugi parameters and θ_5 which is θ measured at 5 kPa.

	$\boldsymbol{\theta_s}$ (cm^3 cm^{-3})	$\boldsymbol{\theta_r}$ (cm^3 cm^{-3})	**log$_{10}$ $\boldsymbol{h_m}$** (cm)	**σ** (-)
Min	θ_5	0.0	1.23	0.8
Max	0.60	0.20	5.42	4.0

Table 2. Description of the tortuosity parameters.

Tortuosity	Description
τ_1	Takes into account the increased path length due to crookedness of the path. When $\tau_1 = 0$ the flow path is perfectly straight down. When τ_1 increases, the flow path is no longer straight but meanders.
τ_2	Theoretically represents the shape of a microscopic capillary tube. The τ_2 parameter is used to estimate restrictions in flow rate due to variations in pore diameter and pore shape. When $\tau_2 = 0$ the shape of the capillary tube is perfectly cylindrical. When τ_2 increases, the tube becomes less perfectly cylindrical, which causes lower connectivity.
τ_3	High porosity soils tend to have large *effective pores*, $\theta_s - \theta_r$, which tend to be more connected than soils with smaller effective pores, which have more dead-ends. When $\tau_3 = 0$ the connectivity is the same between high and low porosity soils. When τ_3 increases the connectivity of the soil increases (Vervoort and Cattle, 2003; Pollacco et al., 2013). Pollacco et al. (2013) found τ_3 to be the least sensitive parameter.

Table 3. Theoretical constraints of the K_{s_bim} model.

Constraint	Explanation
$\theta_s \geq \theta_{s\_mac} >> \theta_r$	Self-explanatory.
$0 < \sigma_{mac} \leq 1.5$	To avoid any unnecessary overlap of θ_{bim} with θ_{bim_mat}.
$1 > \tau_1 > \tau_{1\_mac} \geq 0$	Flow in the macropore domain (larger pores) is expected to be straighter than in the matrix domain (smaller pores) due to reduced crookedness of the path.
$1 > \tau_2 > \tau_{2\_mac} \geq 0$	It is expected that the shape of the 'microscopic capillary tube' of the macropore domain (larger pores) is more perfectly cylindrical than in the matrix domain (smaller pores).
$1 > \tau_3 > \tau_{3\_mac} \geq 0$	The macropore domain has larger pores, and therefore it is assumed that the pores are better connected than the matrix pores.

Table 4. Soil series and classification.

Region	Soil series	No. of horizons		New Zealand classification	Soil taxonomy
		Topsoils	***Subsoils***	***Subgroup***	***Great group***
Canterbury regional study	Eyre	6	8	Weathered Orthic Recent	Haplustepts
	Templeton	9	17	Typic Immature Pallic	Haplustepts
	Wakanui	9	17	Mottled Immature Pallic	Humustepts
	Temuka	9	16	Typic Orthic Gley	Endoaquepts
	Lismore	7	5	Pallic Firm Brown	Dystrustepts
	Hatfield	9	18	Typic Immature Pallic	Humustepts
	Pahau	9	18	Mottled Argillic Pallic	Haplustalf
	Waterton	9	15	Argillic Orthic Gley	Endoaqualfs
Canterbury	Waimakariri		2	Weathered Fluvial Recent	Haplustepts
	Lismore		1	Pallic Orthic Brown	Dystrustepts
	Templeton		6	Typic Immature Pallic	Haplustepts
	Wakanui		2	Mottled Immature Pallic	Humustepts
	Temuka		2	Typic Orthic Gley	Endoaquepts
Manawatu	Hautere		3	Acidic Orthic Brown	Dystrudepts
	Levin		4	Pedal Allophanic Brown	Humudepts
	Levin mottled		4	Mottled Allophanic Brown	Humudepts
	Manawatu		1	Weathered Orthic Recent	Haplustepts
	Paraha		3	Mottled Immature Pallic	Haplustepts
	Westmere		2	Typic Mafic Melanic	Humudepts
Marlborough	Brancott		3	Mottled Fragic Pallic	Haplustepts
	Broadridge		3	Mottled-argillic Fragic Pallic	Haplustalf
	Grovetown		3	Typic Orthic Gley	Endoaquepts
	Raupara		1	Typic Fluvial Recent	Ustifluvent
	Wairau		1	Typic Fluvial Recent	Ustifluvent
	Woodburn		2	Pedal Immature Pallic	Ustochrept
Otago	Dukes		1	Typic Orthic Gley	Endoaquepts
	Linnburn		2	Alkaline Immature Semiarid	Haplocambids
	Matau		4	Typic Orthic Gley	Endoaquepts
	Otokia		1	Mottled Fragic Pallic	Haplustepts
	Pinelheugh		2	Pallic Firm Brown	Eutrudepts
	Ranfurly		2	Mottled Argillic Semiarid	Haploargids
	Tawhiti		2	Pallic Firm Brown	Eutrudepts
	Tima		2	Typic Laminar Pallic	Haplustepts
	Waenga		2	Typic Argillic Semiarid	Haploargids
	Wingatui		2	Weathered Fluvial Recent	Haplustepts
Southland	Waikiwi		2	Typic Firm Brown	Humudepts
	Waikoikoi		2	Perch-gley Fragic Pallic	Fragiaqualfs

Table 5. The $RMSE_{log10}$ reported by using K_{s_bim} and K_{s_uni} models, by stratifying the data with/without texture and layers

Data stratification with	$RMSE_{log10}$		
	K_{s_uni}	K_{s_bim}	K_{s_bim} - K_{s_uni}
All data combined	0.583	0.560	0.023
Loam & clay (texture)	0.577	0.543	0.034
Topsoil & subsoil (layers)	0.450	0.430	0.020

Table 6. Optimal tortuosity parameters of K_{s_uni} and K_{s_bim}.

		N	$RMSE_{log10}$	T_1	τ_2	τ_3	T_{1_mac}	τ_{2_mac}	τ_{3_mac}	$\sigma_{\_mac}$
K_{s_bim}	**Topsoil**	51	0.232	5.007	0.969	0.787	4.734	0.511	0.041	0.322
	Subsoil	181	0.471	6.444	0.859	0.408	3.973	0.642	0.729	1.272
K_{s_uni}	**Topsoil**	51	0.259	5.859	0.967	0.530	-	-	-	-
	Subsoil	181	0.491	6.484	0.854	0.316	-	-	-	-

Table 7. Descriptive statistics of the optimized θ_{mac} (θ_s – θ_{s_mac}), θ_s , h_m and σ Kosugi hydraulic parameters. The bar represents the average value, SD the standard deviation and *N* the number of measurement points.

	N	$\overline{\theta_{mac}}$	SD θ_{mac}	$\overline{\theta_s}$	SD θ_s	$\overline{\theta_{s\_mac}}$	SD θ_{s_mac}	$\overline{lN\ \ h_m}$	SD ln h_m	$\overline{\sigma}$	SD σ	$\overline{K_s}$	SD K_s
		(cm^3 cm^{-3})		(cm^3 cm^{-3})		(cm^3 cm^{-3})		(cm)		(-)		(cm h^{-1})	
Topsoil	51	0.038	0.035	0.48	0.04	0.45	0.04	6.43	1.02	3.00	0.61	167.	101.
Subsoil	181	0.030	0.030	0.42	0.05	0.39	0.06	5.39	1.66	2.64	0.86	19.	42.

Table 8. Summary of the quantile regression fit of the log-transformed residuals.

Quantile	a_0		a_1	
	Estimate	**95% CI**	**Estimate**	**95% CI**
$\tau = 0.025$	–0.476	$[-\infty, -0.44]$	–0.574	$[-0.62, \infty]$
$\tau = 0.500$	0.041	$[-0.036, 0.080]$	0.041	$[-0.093, 0.053]$
$\tau = 0.975$	0.357	$[0.332, \infty]$	0.627	$[-\infty, 0.711]$

Figures

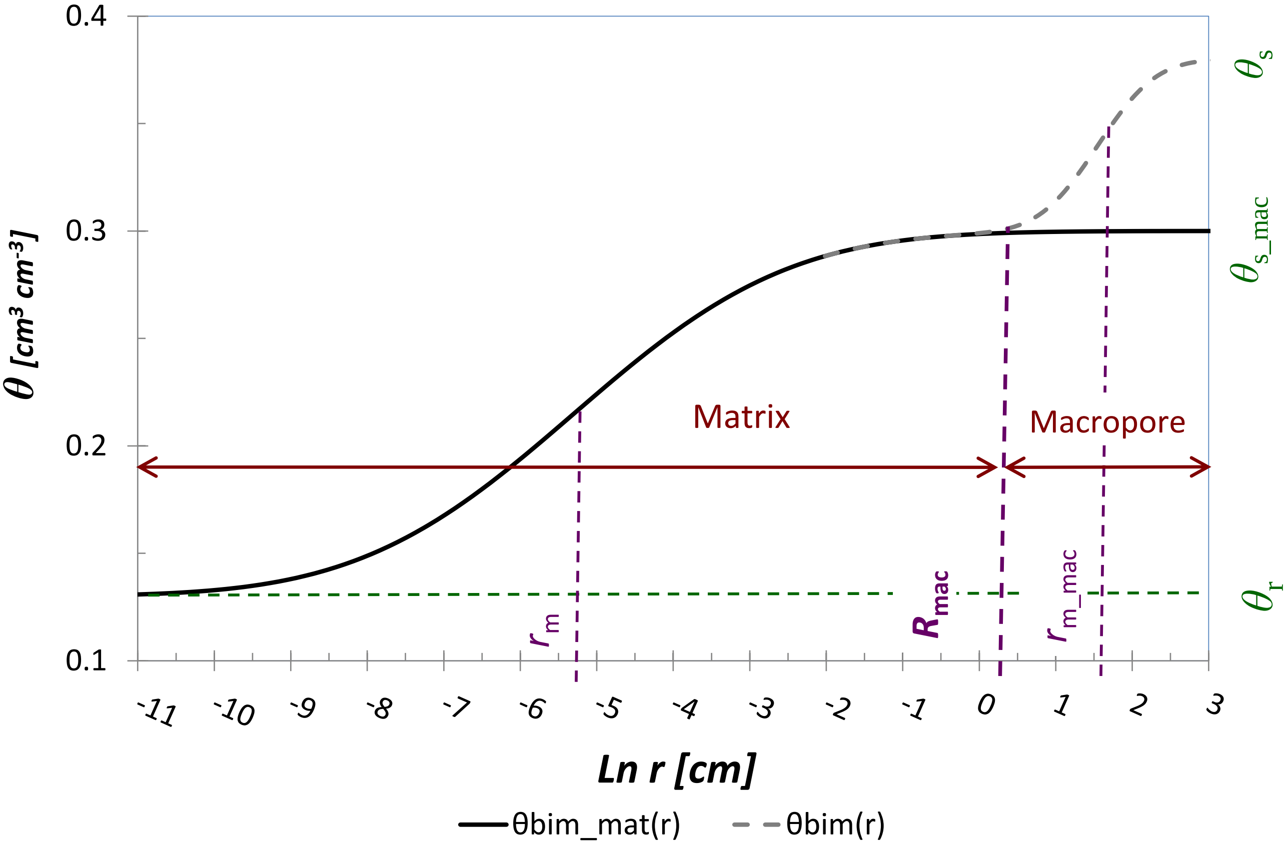

Figure 1. A typical Kosugi θ_{bim} *(r)* (Eq. (10a)) and θ_{bim_mat} *(r)* (Eq. (10b)) with the matrix and macropore domains and the positions of θ_s , θ_{s_mac}, θ_r, r_m, r_{m_mac} , R_{mac} shown.

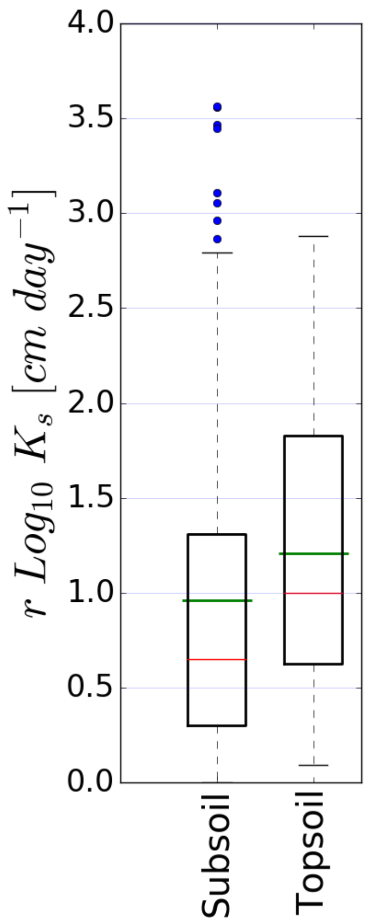

Figure 2. Uncertainty of the standard error of the observed K_s in topsoil and subsoil. The lines in the box show upper and lower quartiles, the median (red), and mean (green). Whiskers show values within 1.5 times the quartile spread; values outside this range are shown as plotted points.

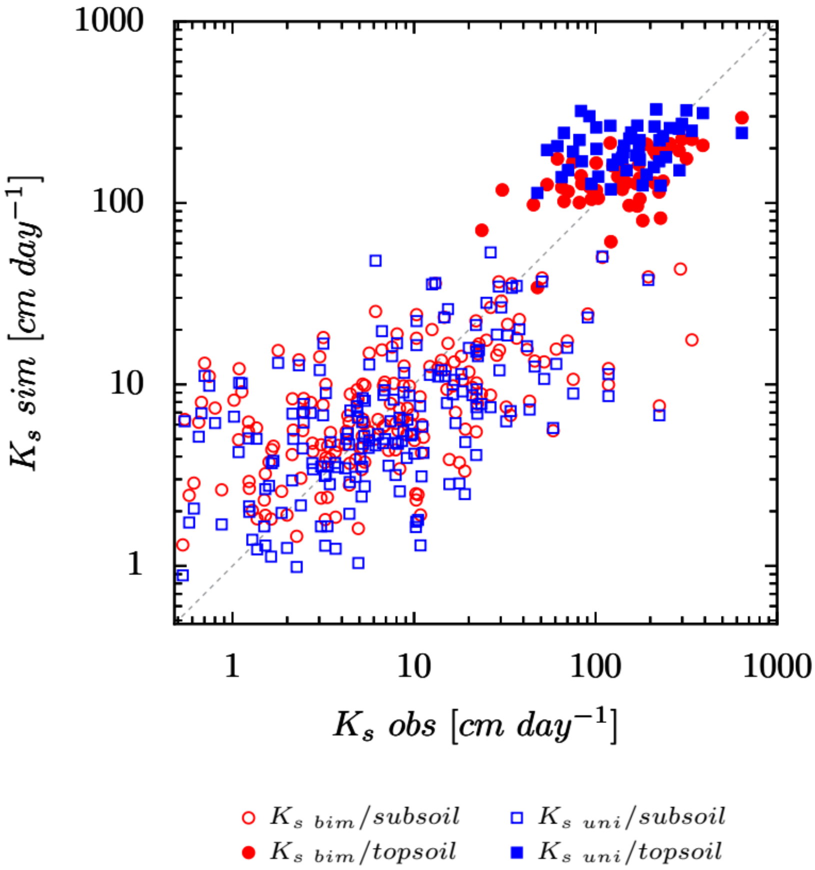

Figure 3. Plot between K_{s_obs} against K_{s_bim} and K_{s_uni} for topsoil and subsoil. The dotted line refers to the 1:1 line.

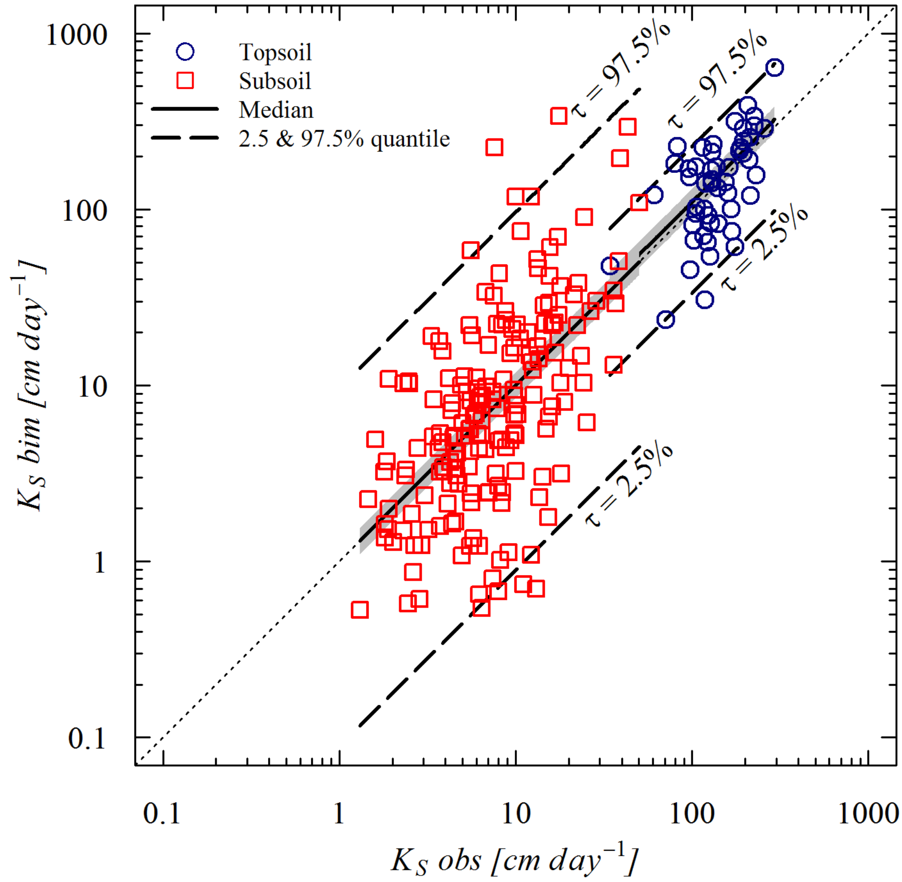

Figure 4. Error of K_{s_bim} plotted against K_{s_obs} for topsoil and subsoil. The solid line refers to the median line for each group, the dashed line refers to the upper or lower 95% confidence interval lines, the dotted line refers to the 1:1 correspondence line, and the shaded region is the 95% confidence interval of the median estimate